Intraspinal Microstimulation using Cylindrical Multielectrodes

Sean Snow, *Member, IEEE*, Kenneth W. Horch*, *Member, IEEE*, and Vivian K. Mushahwar, *Member IEEE*

***Abstract*—A cylindrical multielectrode system specifically designed for intraspinal microstimulation was mechanically and electrically evaluated in the ventral horn of the feline lumbo-sacral spinal cord. Electrode insertions proved to be straight as evaluated from radiographs. Impedances were measured in situ and force recruitment curves from quadriceps muscles were collected over a wide range of stimulus parameters. For a given charge, higher current amplitudes produced greater forces than proportionally longer pulse durations, indicating that charge is not the sole indicator of evoked force in applications utilizing electrical stimulation. Overlap measurements for calculating current-distance constants were collected at a variety of current amplitudes, electrode pair separations, and pair orientations in the spinal grey matter. Forces obtained in the majority of these trials demonstrated an order effect, presumably due to asymmetric neuronal connectivity within the spinal cord. In the cases showing no order effect, the dorso-ventral electrode pair orientation yielded a higher average current-distance constant (278 $\mu A/mm^2$) than either the medio-lateral or rostro-caudal electrode pair orientations (197 $\mu A/mm^2$). Specifications of an array of cylindrical multielectrodes for use in future intraspinal microstimulation prostheses were updated.**

***Index Terms*—Current distance constants, electrode array, spinal cord stimulation.**

I. Introduction

A quarter of a million persons in the United States are currently disabled due to spinal cord injuries [1]. Much research has focused on restoring limb function in these individuals by activating the paralyzed muscles either through the peripheral or the central nervous system [2]–[8]. Peripheral stimulation can require complex multiple surgeries since the electrodes are implanted in up to 16 different locations [9]. On the other hand, an electrical prosthesis implanted in the central nervous system may offer single point implantation, improved recruitment characteristics, a more mechanically stable implant site, and useful access to neuronal networks for recruiting complex patterns of movement. Previous studies of intraspinal microstimulation (ISMS) have shown that ISMS results in stable, gradable recruitment of force in the muscles of the lower limbs during chronic experiments [10], provides better control than peripheral nerve cuff stimulation [11], and is capable of producing complex movements attributable to intrinsic neuronal networks in the spinal cord [12], [13].

These studies used fine wires as intraspinal electrodes. Each electrode provided a single stimulation site per insertion and, when arrayed, offered a two-dimensional distribution of stimulation sites within the motor pool. A new electrode system is needed that would provide multiple stimulation sites for each insertion and thereby yield a three-dimensional distribution of electrode locations. The electrodes must also minimize the tissue displaced by the implantation and be capable of being inserted without bending.

Current multielectrode systems were considered for use with ISMS but are not suitable for the spinal cord environment. Electrode systems such as the Utah Slanted Electrode Array [14] could be redesigned to offer a three-dimensional distribution of electrode sites, constrained to one electrode per shaft, but are not yet long enough to access the motor pools as deep as 4.5 mm below the cord surface. We have found that true three-dimensional electrode arrays built using planar silicon, such as those produced at the University of Michigan, break easily during insertion if not aligned perfectly and are not stiff enough to penetrate deep into the ventral horn without deviating. Finally, silicon-based microfabricated electrode arrays, which have been stiffened by electroplating, provide for electrode site fabrication on only one side of the electrode and result in large electrode volume per electrode site area [15]. An alternative electrode array was suggested that would be comprised of individual shafts, each containing multiple electrode sites [16]. These cylindrical multielectrodes have been constructed using microfabrication techniques and have been proven to be reliable in delivering charge during benchtop testing [17].

This paper reports on the *in vivo* characteristics of cylindrical multielectrodes placed in the lumbar spinal cord, with emphasis on insertion characteristics, impedance stability, recruitment of force in the quadriceps muscle, and stimulation current-distance constants. These data were combined to determine the optimal spatial distribution of electrode sites within the quadriceps motoneuron pool.

II. Methods

A. Experimental Setup

Seven adult, female cats were used in this study. Anesthesia was induced using 40 mg/kg of sodium pentobarbital administered intraperitoneally and maintained to effect using 1:10 di-

Manuscript received October 4, 2004; revised March 27, 2005. This work was supported in part by the National Institutes of Health through the National Institute of Neurological Disorders and Stroke (NINDS), in part by the Canadian Institutes for Health Research (CIHR), and in part by the Alberta Heritage Foundation for Medical Research (AHFMR). *Asterisk indicates corresponding author.*

S. Snow, was with the Department of Bioengineering, University of Utah, Salt Lake City, UT 84112 USA (e-mail: s.snow@m.cc.utah.edu).

*K. W. Horch is with the Department of Bioengineering, 50 S. Central Campus Dr., University of Utah, Salt Lake City, UT 84112 USA (e-mail: k.horch@utah.edu).

V. K. Mushahwar is with the Department of Biomedical Engineering, University of Alberta, Edmonton, AB T6G 2S2, Canada (e-mail: vivian.mushahwar@ualberta.ca).

Digital Object Identifier 10.1109/TBME.2005.857638

lution of sodium pentobarbital in saline delivered through the jugular vein. Blood pressure and heart rate were monitored via the carotid artery.

A medial thigh incision provided access to the extensor branch of the femoral nerve in one leg and a bipolar cuff electrode, with a 3 mm interelectrode separation, was installed. Two sutures were tied around the electrode to secure it in place around the nerve and the skin incision was sutured shut. The hip and hind legs were stabilized and prepared for force measurements as previously described [16]. Both patellas were detached distally and sutured to force transducers (ISMS leg = model SM-25, cuff leg = model SM-50, Interface Inc.) to allow for the measurement of isometric quadriceps forces.

Whole nerve, twitch recruitment curves were collected by sampling the output of the force transducers at 4 kHz with a digital data acquisition system during stimulation with 300 μs long, monophasic pulses applied to the cuff electrode by a Neurolog stimulator (NL800, Digitimer, Ltd.). Amplitudes ranged from threshold to supramaximal. Tetanic contractions were then digitized while stimulating with the same pulse parameters at 50 Hz for 1 s. After the cuff stimulations were completed, a laminectomy was performed on vertebrae L4 and L5. Using a fine wire electrode, stimuli were delivered to identify the rostral and caudal borders of the region which provided isolated quadriceps recruitment in the leg without the cuff electrode. Three electrode shafts [17] were implanted in the rostral half of the quadriceps region 1 mm inside the rostral border and three additional electrode shafts were implanted in the caudal half of the quadriceps region 1 mm from the caudal border.

Each electrode shaft was 4.4 mm long, 85 μm in diameter, and contained four, iridium-plated electrode sites with 400 μm between each site. Each electrode site was 70 μm high along the direction of the shaft and 140 μm long around the 267 μm circumference of the shaft. A 14 gauge needle served as the return electrode and was inserted into the paravertebral musculature.

A custom-built stimulation system provided current pulses to as many as 32 electrode sites. Computer-controlled digital outputs selected the address of the channel to receive stimulation and a digital-to-analog converter delivered the signal voltage to the selected voltage-controlled current source. Current pulse durations and amplitudes were calibrated prior to the experiment. Each current source was capacitively coupled to an electrode site to block DC currents. All stimuli were biphasic, cathodic-first, 300 μs long, and charge-balanced with anodic pulses of equal amplitude and equal duration, unless otherwise noted.

Threshold currents were determined for all electrode sites. Of these, four contiguous sites with thresholds ranging from 7 to 20 μA were selected from each end of the pool and used in collecting recruitment curves and overlap data.

B. Stimulation Parameters

Several *in vivo* properties were tested and each required specific stimulus parameters. Each stimulus was delivered more than 60 s after the previous stimulus to minimize the effects of fatigue.

1) Impedance: Electrode impedances were periodically measured throughout the experiment and monitored for any large increases possibly indicating material loss at the electrode interface. Limitations of the stimulation system precluded using sinusoidal current trains to measure impedance. Instead, the impedance of each electrode site was measured by applying a 100-μA-amplitude, 300-μs-duration current pulse and measuring the maximum voltage difference between the output of the stimulation system and the return electrode using an oscilloscope (123, Fluke Corp.). The impedance was recorded as the maximum voltage divided by the current pulse amplitude. This impedance measurement consisted of both the interfacial impedance of the electrode site in addition to the impedance of the bulk material between the stimulation electrode and the return electrode. Information about electrode impedance *in vitro* using 1 kHz currents can be found in the companion paper [17].

The impedances of 12 sites were measured in one animal under three conditions: on top of the spinal cord submerged in saline, in the spinal cord at the beginning of the experiment, and in the spinal cord 14 h later at the conclusion of the experiment.

2) Recruitment: Force recruitment curves were collected to determine how well muscle activation could be graded. A total of 42 stimulation sites were used in five animals to collect twitches for pulse amplitude modulated recruitment curves using 300-μs-long pulses with currents ranging from threshold to 300 μA.

In the other two animals, 12 additional stimulation sites were used for acquiring two types of recruitment curves: pulse amplitude modulated with a fixed pulse width and pulse width modulated with a fixed pulse amplitude. This was done to determine if charge was the sole factor required to predict force. Pulse amplitude recruitment curves were collected at 200, 300, and 500 μs for charges ranging from 3 to 60 nC (the 500 μs recruitment curve went up to 75 nC). Pulse width recruitment curves were collected at 50, 100, and 200 μA from 3 to 60 nC.

In order to compare the tetanic forces between whole nerve stimulation and ISMS, trains of 90 nC pulses were delivered at 50 Hz for 1 s through 24 stimulation sites comprised of a subset of the 42 sites used to collect pulse amplitude recruitment curves and the 12 sites used to collect both pulse amplitude and pulse width recruitment curves. Six of the 24 electrode sites were also used to produce tetanic forces using trains of 30 nC pulses.

Strength-duration curves were collected using six electrode sites in one animal to determine the chronaxie and rheobase of the neurons lying closest to each stimulation site. Methods for finding the rheobase, the lowest stimulating current, and the chronaxie, the pulse duration at twice the rheobase current, are summarized by Tehovnik [18]. Pulse widths were varied from 15 to 1200 μs. For each pulse width, the threshold current was determined as the minimum current required to elicit a 75 mN force above baseline in 50% of the trials.

For each force trace, the data were first smoothed using an eight point running average, then the baseline force was calculated by averaging forces 150 ms before the stimulus. Maximum forces were calculated by subtracting the baseline force from the peak force.

3) Overlap: In order to determine the current spread characteristics within the spinal cord, two electrodes with fixed positions were used in conjunction with overlap measurements. Overlap testing first required the determination of the refractory period of neurons at each electrode site. This was done using two types of stimulus pairs: immediate charge balanced and delayed charge balanced.

Immediate charge balanced stimulus pairs consisted of a 300 μs cathodal pulse followed immediately by a 300 μs anodal charge balancing phase, the interstimulus interval, and finally a second biphasic stimulus. Delayed charge balanced stimulus pairs consisted of a cathodal pulse, the interstimulus interval, a second cathodal pulse, a 100 μs pause, and finally a 600 μs long anodal pulse that balanced the charge for both cathodal pulses. After the characteristics of the refractory period were determined, an interstimulus interval was chosen that fell near the end of the absolute refractory period (typically 100 μs). This point in the refractory period was chosen to avoid possible activation of fibers beginning to recover from refractoriness while minimizing any residual depolarization in fibers that did not reach threshold from the first stimulus. This interval and the stimulus configurations described above were used when testing for current spread.

In order to determine the range of current spread, the following relationship between current and the distance at which the stimulus activates neurons was used

$$\text{Distance} = \left(\frac{\text{Current}}{K}\right)^{\frac{1}{2}} \tag{1}$$

where K is the current-distance constant [18]. Whereas previous studies utilized a recording electrode near the neuron to determine activation and varied the position of the stimulating electrode [19], our study used two stimulating electrodes and overlapping regions of stimulation. For this method, overlap was calculated by

$$\text{Overlap} = \frac{F_a + F_b - F_{\text{refrac}}}{F_{\text{refrac}}} \tag{2}$$

where F_a and F_b are the forces resulting from stimulation through each electrode separately, and F_{refrac} is the force resulting from refractory mode stimulation [16], [20]. Refractory mode stimulation consisted of delivering a current pulse to one site and then delivering a current pulse to the second site while the neurons stimulated by the first stimulus were still in their refractory period. The refractory mode stimulation was repeated with the order of the stimuli reversed to determine the effect of stimulation order. In two of the three animals tested, the pulses were charge balanced following the cathodic pulse. In one of the animals, the delivered pulses were monophasic. After the forces were collected, the data were processed to calculate overlap and further processed to generate a value for K.

Calculation of K required knowing the stimulation current amplitudes, the calculated overlap, and the separation between the stimulation sites (measured from radiographs). By combining (1) and (2), and solid geometry modeling (see Appendix), the separation between stimulation sites and the currents were used to solve for K. The model was based upon the assumptions that the stimulated region is spherical with a homogeneous neural distribution and that, for each neuron exhibiting overlap, the neuron's sites of activation are either the same for both electrodes or located near to one another relative to the electrode separation distance.

C. Anatomy

At the conclusion of the experiment, the cat was deeply anesthetized with sodium pentobarbital. The skin was closed over the laminectomy for protection of the spinal cord during perfusion. Palay's (formaldehyde) fixative was administered via the left ventricle of the heart and the body was refrigerated overnight. The following day the laminectomy was widened and the spinal cord was removed. Two, 10 mm long segments of the spinal cord, each containing three electrode shafts, were trimmed out of the cord. Each of these tissue samples was x-rayed in both lateral and axial views. Radiographs were then scanned and analyzed using image processing software to determine the distances between electrode sites and if there was any curvature of the electrode shafts. Electrodes were then removed and the tissue was sectioned at 50 μm. Sections were backlit and photographed to determine the location of the electrode sites relative to the ventral horn boundaries.

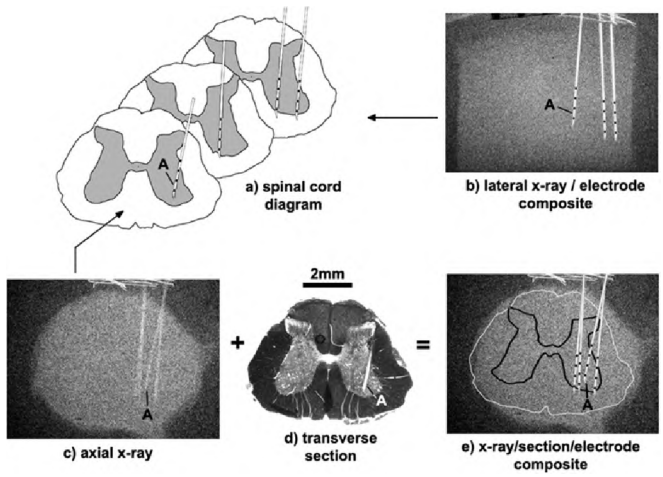

Fig. 1. Example of anatomical image processing. A perfused spinal cord segment containing the electrodes was removed from the animal and divided into two halves, each containing 3–4 electrode shafts. X-ray images, (b) and (c), were taken with the electrode shafts in place. The electrodes were then removed and the spinal cord segments were sectioned and photographed (d). Using image processing software, a digital representation of an electrode was scaled and superimposed upon each electrode shadow in the radiograph (b). An image of the tissue section was mated with the digital representation of the electrode such that the electrode tract lined up with the digital electrode. The grey and white matter was outlined and superimposed on the radiograph with the electrode graphics (e).

III. Results

A. Electrode Insertion

A total of 46 electrode shafts were inserted in six animals. All radiographic electrode shaft shadows were straight to within 100 μm over the 4 mm length on both views, i.e., there was no measurable curvature of the implanted shafts. A sample of the image processing is shown in Fig. 1. The electrode sites for the first experiment were found to be located at the grey-white matter border and, for this reason, were excluded from some results.

B. Impedance

Impedances were measured in one animal from 16 sites on eight shafts, between each site and the return electrode. This was first done while the electrodes were lying on top of the spinal cord submerged in saline. The average impedance was 18.4 ± 0.4 kΩ (mean $\pm$ s.e.). After the same electrodes were inserted into the spinal cord, the average impedance increased to 55 ± 3 kΩ. After 14 hours of testing, the average measured impedance was reduced (t-test, $p = 0.01$) to 46 ± 2 kΩ.

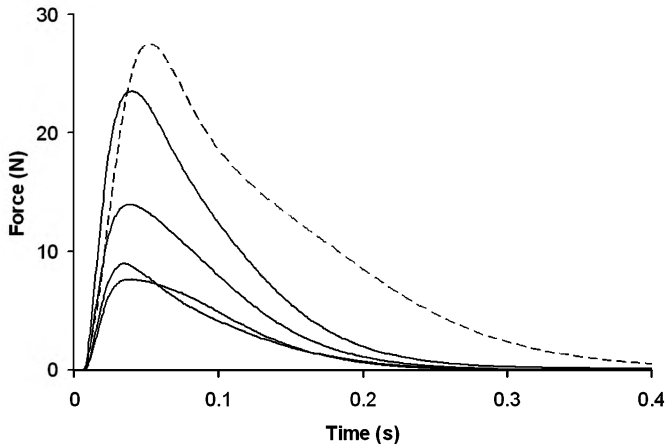

Fig. 2. Typical muscle twitches elicited by single 300 μA, 300 μs pulses through whole nerve stimulation (dashed line) and ISMS (solid lines). Four twitches are shown for ISMS, each corresponding to a different electrode site on a different electrode shaft, since ISMS resulted in a variety of twitch forces. The lowest maximum force twitch took longer to relax and would seem to indicate that a higher percentage of slow twitch fibers were activated.

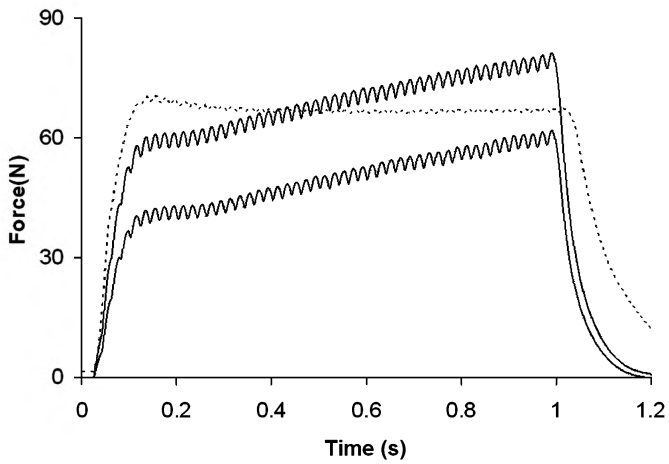

Fig. 3. Typical muscle forces resulting from tetanic stimulation (300 μs, 300 μA, 50 Hz) of both whole nerve stimulation (dashed line) and ISMS (solid lines). Increasing tetanic forces during the period of stimulation were observed in almost all ISMS 50 Hz stimulation trials, indicating the recruitment of high proportions of slow muscle fibers.

C. Recruitment

1) Responses: Stimulation with monophasic pulses through the cuff electrode and biphasic pulses through the intraspinal electrodes resulted in muscle twitches as shown in Fig. 2. Stimulating at 50 Hz resulted in tetani as shown in Fig. 3. For the ISMS tetanic forces, the forces steadily increased during the 1 s stimulation. This increasing tetanic force was seen with 22 of 23 intraspinal electrode sites, but only once in seven maximal cuff stimulations.

2) Relative Force Levels: The maximum twitch force and maximum tetanic force from each intraspinal electrode site was averaged, with results shown in Table I. In addition to these forces resulting from 90 nC stimuli, force levels were also determined for 30 nC stimuli.

The average twitch force generated from intraspinal delivery of a 90 nC stimulus was much smaller than that from whole nerve stimulation (14.2 versus 31.8 N, t-test, $p < 0.001$), but the average tetanic forces for ISMS and whole nerve stimulation were not statistically different from each other (81.3 versus 97.3 N, t-test, $p > 0.3$). For whole nerve pulse amplitude recruitment curves collected using twitches, the forces plateaued in 100% of the curves, with a plateau defined as the 90 nC force being less than or equal to the force collected at 60 nC. ISMS pulse amplitude recruitment curves showed a plateau in only 24% of the curves.

TABLE I
FORCE LEVELS OBTAINED FROM ISMS AND WHOLE NERVE (CUFF) STIMULATION

	30 nC Stimulus		90 nC Stimulus	
	Twitch Force	Tetanic Force	Twitch Force	Tetanic Force
ISMS	3.42 ± 0.50 (42)	31.3 ± 7.4 (6)	14.2 ± 1.4 (42)	81.3 ± 6.6 (24)
Cuff	15.3 ± 6.5 (4)	21 ± 14 (4)	31.8 ± 2.7 (5)	97.3 ± 13.8 (6)

Forces (N) are reported as mean ± standard error with the number of data points listed in parentheses.

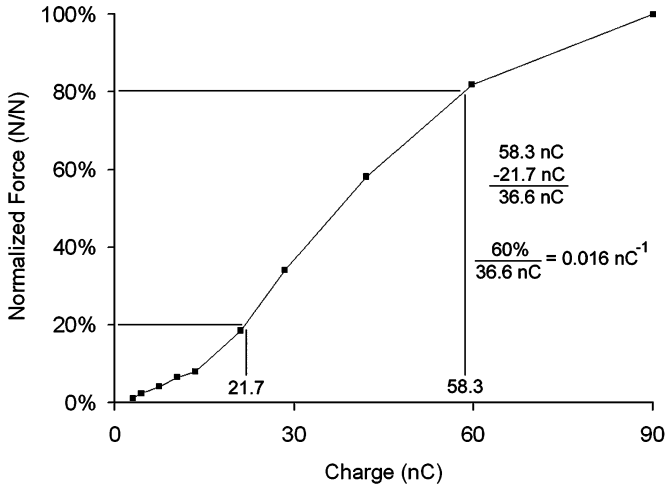

Fig. 4. Calculation of recruitment curve slope using the 20/80 method on a typical recruitment curve. The charge associated with the force at 80% of maximal force was determined by interpolation and the same method was used to determine the charge for the 20% level. The charge at the 20% level was subtracted from the charge at the 80% level. The difference represented the charge covering 60% of the force range. The recruitment curve slope was calculated by dividing 60% by 36.6 nC, resulting in 0.016 nC^{-1}.

The forces elicited from the caudal half of the cord were greater than those generated from the rostral half (t-test, $p = 0.001$). When the 90 nC stimulus twitch forces for each intraspinal site were normalized by the maximum force resulting from 90 nC stimuli in that animal, stimulation in the caudal half of the pool resulted in an average normalized force of 0.73 ± 0.06 (mean ± s.e.) compared to 0.45 ± 0.05 from the rostral half. Tetanic contractions gave similar results: rostral ISMS produced 72% of the force seen with the cuff while caudal stimulation produced 107% of the force produced from the cuff (20 measurements in 4 animals, t-test, $p < 0.02$).

3) Recruitment Curves: A total of 4 cuff electrode and 32 intraspinal electrode recruitment curves were collected in four animals. Slopes of the recruitment curves were calculated using 20% and 80% levels (Fig. 4) to avoid the asymptotic regions at both the low and high ends of force. The average ISMS recruitment curve slope ($0.0186 \pm 0.0010\ \mathrm{nC}^{-1}$) was 2.9 times shallower than the average cuff electrode recruitment curve slope ($0.0533 \pm 0.0055\ \mathrm{nC}^{-1}$). Normalizing the data by dividing each ISMS recruitment curve slope from a given experiment by the cuff recruitment curve slope from the same animal, to insure that the

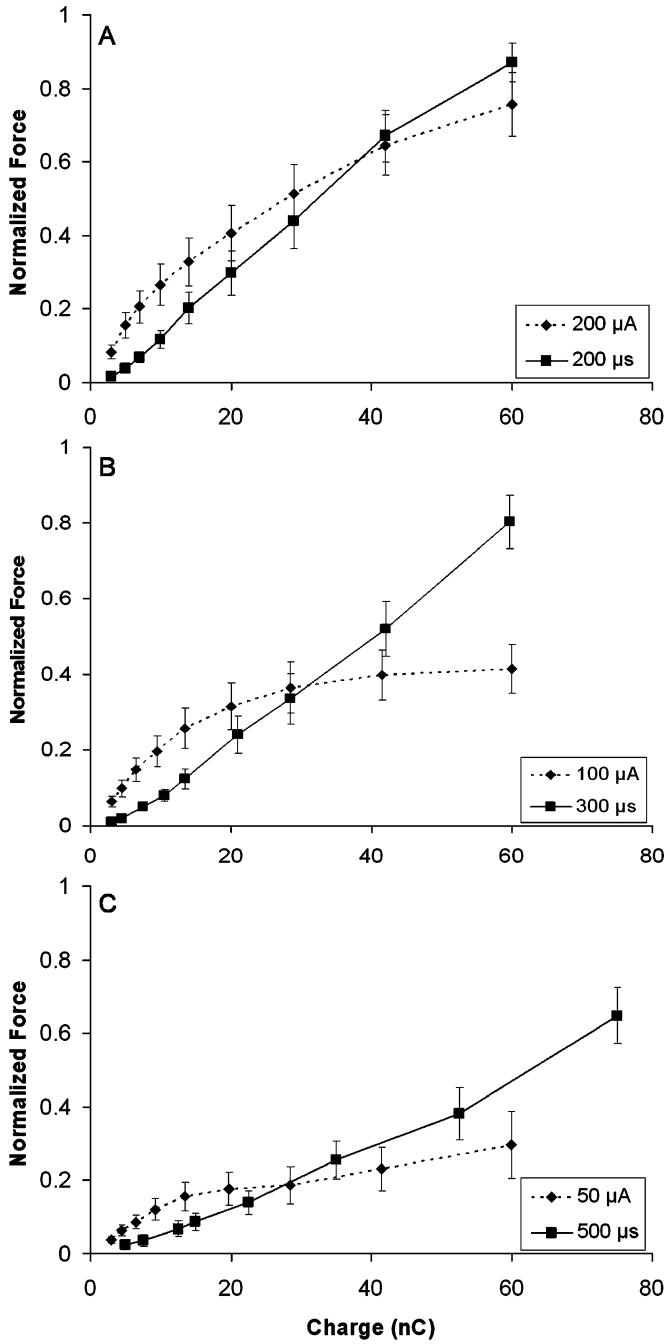

Fig. 5. Pulse amplitude modulated recruitment curves and pulse width modulated recruitment curves. Pulse amplitude recruitment curves were collected at 200, 300, and 500 μs. Pulse width recruitment curves were collected at 50, 100, and 200 μA. Each of 12 electrode sites was tested using the six different stimulation parameters. For each electrode site, the force values for all six conditions were normalized to the highest force recorded for the six conditions. Error bars represent the standard error.

results were not dominated by data from one experiment, gave equivalent results: a mean ISMS-to-cuff ratio of 0.36 $\pm$ 0.03.

For 12 electrode sites, three pulse amplitude modulated recruitment curves with pulse widths of 200, 300, and 500 μs and three pulse width modulated recruitment curves with pulse amplitudes of 50, 100, and 200 μA were collected. For each electrode site, all recruitment curves were normalized by the maximum force obtained from the six recruitment curves to correct for differences in muscle strength between animals. Fig. 5

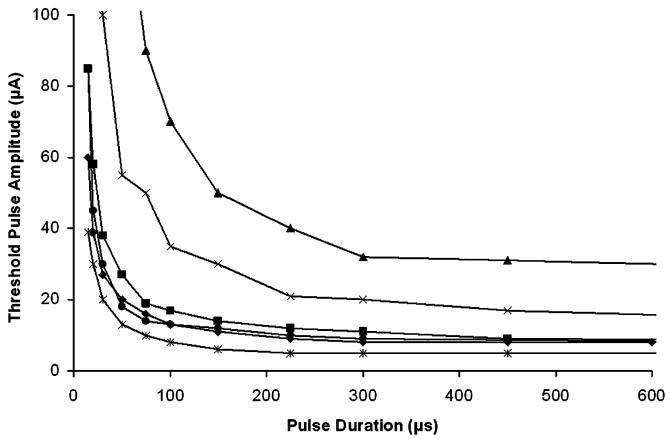

Fig. 6. Strength-duration curves collected for an electrode site on each of six electrode shafts. The pulse amplitude required to exceed threshold, defined as 75 mN above baseline, was recorded as a function of pulse duration.

shows all 12 sites averaged together, resulting in six recruitment curves. For presentation, the largest force pulse amplitude modulated recruitment curves (200 μs stimulus duration) have been grouped with the largest force pulse width modulated recruitment curves (200 μA stimulus strength), and the smallest force pulse amplitude modulated recruitment curves (500 μs) were grouped with the smallest force pulse width modulated recruitment curves (50 μA). Each pair of averaged recruitment curves crossed one another at the appropriate charge (the product of the fixed pulse width and the fixed pulse amplitude). In each case, the pulse width modulated recruitment curves delivered higher forces at charges below the crossover point and the pulse amplitude modulated recruitment curves produced larger forces above the crossover point.

4) Strength-Duration Curves: Threshold current levels were determined for six electrode sites at pulse widths that varied between 15 and 1200 μs. The results (Fig. 6) show that the rheobase was reached below 600 μs. The average rheobase was 11 $\pm$ 4 μA (mean $\pm$ s.e.) and the average chronaxie was 120 $\pm$ 50 μs.

D. Overlap

Overlap was measured by stimulating with a pair of electrode sites delayed by 100 μs, an interval determined to be in the absolute refractory period of the neurons and in agreement with a detailed study of refractory period in peripheral nerve [20]. Both immediate charge balancing and delayed charge balancing stimulation methods were used, but there was no difference between the two methods (t-test, $p = 0.91$). Current-distance constants (Ks) were computed for 26 electrode site pairs in three animals, with each pair tested at three current levels and both orders (A, B and B, A) resulting in 120 values of K.

Order effect was considered present if the forces resulting from first stimulating site A and then site B were statistically different (t-test, $\alpha = 0.01$ or $\alpha = 0.05$) from the forces resulting from stimulating site B followed by site A. This effect was seen in 62% ($\alpha = 0.01$) or 73% ($\alpha = 0.05$) of the trials. K values were retained only if they resulted from overlap measurements that were greater than zero and showed no evidence of order effect.

TABLE II
K VALUES ($\mathrm{mA/mm^2}$) WITH OVERLAP ORDER EFFECT REMOVED AT TWO DIFFERENT α LEVELS

Electrode pair orientation	$\alpha = 0.01$	$\alpha = 0.05$
Medio-lateral / Rostro-caudal	197 ± 18 (24)	177 ± 23 (16)
Dorso-ventral	278 ± 31 (15)	273 ± 35 (10)
t-test, ML/RC vs. DV	p = 0.018	p = 0.036

K values are reported as a mean ± standard error with the number of data points listed in parentheses.

Four factors were analyzed for correlation with the value of K: cord half, current level, electrode pair separation, and electrode pair orientation. There was no dependence of K on cord half (rostral half versus caudal half, t-test, $\mathrm{p} = 0.33$), current level (t-test, $\mathrm{p} = 0.8$), or electrode pair separation (t-test, $\mathrm{p} = 0.55$). There was no difference in those pairs oriented medio-laterally (ML) versus rostro-caudally (RC) (t-test, $\mathrm{p} = 0.58$) and, therefore, these two groups were combined. Dorso-ventrally oriented pairs resulted in a higher average K than those of the ML/RC group (Table II).

IV. DISCUSSION

These experiments had four goals: evaluating insertion of the electrodes, measuring their impedances, comparing quadriceps contraction forces resulting from ISMS and whole nerve stimulation, and determining current-distance constants in the spinal cord.

A. Electrode Insertion

Radiograph analysis of the electrode positions and curvature was possible due, in part, to the dense material used. The gold circuit traces on the cylindrical multielectrodes, having a high atomic number (79), readily absorbed x-rays and provided sufficient contrast for visualization and analysis. Of the shafts tested, 45 were inserted easily and all 46 were inserted straightly (as verified by radiographs). For the one shaft that required a higher insertion force, a subsequent analysis of the tip via microscopy proved the tip was intact but provided no clues as to why the insertion was more difficult.

B. Impedance

Impedances between the electrode site and the return electrode increased after the electrodes were inserted into the spinal cord. This is presumably due to the conductivity differences of the tissue (containing myelin and cell membranes) versus saline. Further testing is required to quantify the contribution of the bulk material surrounding the electrode site to the measured impedance. After 14 hours of intermittent stimulation, the measured impedances were reduced. It is possible that this was due to activation of the electrode interfacial material of iridium oxide or through a reduction in the impedance of the bulk material by some mechanism such as tissue inflammation.

C. Recruitment

1) Responses: The twitch response elicited through nerve cuff stimulation was nearly three times that of ISMS for a fixed charge. Some of the ISMS twitches showed slower relaxation times (Fig. 2). This could indicate either activation of a high proportion of slow motor units by the latter, or the late, reflexive activation of additional muscle fibers. The argument for slow motor units is supported by the results from tetanic stimulations. The ISMS tetanic forces displayed increasing forces (Fig. 3) over the duration of the 1 s pulse train whereas the cuff-stimulated tetanic force slowly decreased after the peak was reached. This increasing force has been documented by Burke in the soleus muscle of a cat [21] and attributed to activation of high proportions of slow motor units [22]. Direct comparisons of quadriceps muscle fibers activated through ISMS versus whole nerve stimulation through a cuff demonstrated that ISMS preferentially recruits type I and type IIa muscle fibers, while fibers activated by whole nerve stimulation are predominantly type IIb and IId [23].

2) Recruitment Curves: Comparison of cylindrical multielectrodes and tungsten electrodes showed that the recruitment curve slopes were statistically the same (t-test, $\mathrm{p} > 0.1$). Cylindrical multielectrode stimulation resulted in an average recruitment curve slope of $0.019 \pm 0.001\ \mathrm{nC^{-1}}$ (mean ± s.e.) compared to slopes resulting from tungsten electrodes of $0.074 \pm 0.028\ \mathrm{nC^{-1}}$ [24]. Compared to the previously used tungsten electrodes, cylindrical multielectrodes proved similarly easy to implant, provided greater force levels, and similar recruitment curve slopes.

When comparing the recruitment curve slopes resulting from ISMS and whole nerve stimulation, ISMS produced recruitment curve slopes 2.8–2.9 times shallower than whole nerve stimulation. This shallower recruitment curve is an important benefit of ISMS since it allows a neural prosthetic system a finer degree of force modulation in that muscle.

Surprisingly, our results showed that the force levels of the recruitment curves were affected not only by the charge injected, but also by other stimulation parameters as well. The results shown in Fig. 5 were obtained using the same stimulation system through 12 intraspinal electrodes in two animals. To eliminate the possibility that these results stemmed from a problem with the stimulator or electrodes, a new spinal cord location was implanted with a microwire. Pulse-amplitude and pulse-width modulated stimuli were delivered through the microwire using a Neurolog stimulator (NL800, Digitimer, Ltd.) and produced similar results.

The stimulation parameters selected for pulse amplitude modulated recruitment curves and pulse width modulated recruitment curves were limited by the 300 μA maximum current of our custom-designed stimulation system. Given this 300 μA maximum, 60 nC pulses could only be produced by constraining the pulse width to 200 μs or above. This pulse duration was 67% greater than the average chronaxie found in our experiments, despite the recommendation by Tehovnik that pulse widths should be shorter than the chronaxie [18]. By considering the pulse width modulated recruitment curves collected at 50, 100 and 200 μA, Fig. 5 shows that the shorter the pulse width used, the higher the resulting force. In future studies, the stimulus parameters should be adjusted to include pulse widths as short as 75 μs and pulse amplitudes as high as 800 μA (which should still be in the safe limit for stimulation [25]).

Given the stimulus parameters used in this study, stimulation efficiency guidelines can be suggested. This may be useful since microelectrodes are often limited by their charge delivery capacity. In the low end of the charge range (0–30 nC), the highest

force per unit charge was found when using pulse width modulation at 200 μA (Fig. 5). For the high range (30–60 nC), the highest force per unit charge was obtained using either pulse width modulation at 200 μA or using pulse amplitude modulation at 200 μs. If the goal were to operate on the most linear recruitment curve over the full range of charge delivery, the recommended stimuli would be pulse width modulation at 200 μA or pulse amplitude modulation at 200 or 300 μs. These same stimulus parameters would be recommended if maximum force generation were desired.

D. Overlap

An order effect, i.e., differences in the forces resulting from stimulating with electrode A then B versus B then A, was seen in 60%–75% of the cases and over a wide range of test conditions. It was seen for both biphasic and monophasic pulses, immediate charge balanced stimuli (with either no or a 100 μs interphase interval), and delayed charge balanced stimuli, across all five animals tested, across a wide range of current levels, and with several pair separation distances.

One possible explanation of order effect posits that individual neurons were being activated at widely disparate (relative to the spacing between the electrodes) points by the two electrodes [26]. However, unless the induced action potentials did not invade the whole cell, making it refractory, this should not matter in our case. Moreover, we found that electrode pairs placed within the quadriceps pool but spaced 10 mm apart did not show any signs of overlap.

A more plausible explanation relies on asymmetric networks (either inhibitory or excitatory) within the spinal cord. For example, if the neurons stimulated in zone A monosynaptically inhibit those in zone B, the stimulation of A then B could result in the inhibition from A arriving at B at the same time the stimulation to B is delivered. This would result in the production of the full force from A and a partially inhibited force from B. If the inhibitory connection from B to A were polysynaptic or nonexistent, stimulating B and then A would allow the stimulation of A before the inhibition (if any) from B arrives at A, thereby allowing full stimulation of A and B. A difference in forces indicates order effect. Once this observation is better understood, order effect may become useful in deducing the arrangement of neuronal networks within the spinal cord.

In 61 overlap measurements in which the calculated overlap was greater than zero and contained no order effect, the current used to make the measurements ranged from 30 to 135 μA. Using this current range and the average K (232 $\mu\mathrm{A}/\mathrm{mm}^2$), the stimulation radii can be calculated at between 360 and 766 μm. This is close to the range of 480 to 1000 μm for 30 to 135 μA currents compiled by Ranck [27]. It is also close to the radii of 250 to 500 μm for currents ranging from 50 μA to 100 μA predicted by Lemay [13] and estimated by Mushahwar [16].

RC- and ML-oriented electrode pairs resulted in Ks that were statistically different from those obtained with dorso-ventrally (DV) oriented electrode pairs. The difference in the K_s is due to either anisotrophic morphology of the motor pool or is related to the DV orientation of the electrode. In past studies, DV orientations have been shown as the best method for accessing the motor pools. If this method is used in future applications, the question of which factor affects K becomes moot and future electrode spacing should be adjusted for the difference in current spread. The 46% higher K observed in the DV orientation corresponds to a 21% lower current spread and, therefore, specifies a need to place electrodes closer together in the DV direction than in the RC or ML directions.

Previous specifications for an electrode array can be updated using the data from this study [16]. Based on the maximal twitch force generated with intraspinal electrodes (14.2 N) as compared to cuff electrodes (31.8 N), an array must provide at least 2 sites within the quadriceps pool to produce the twitch force obtainable with whole nerve stimulation. But using twitches may be an unfair measure for comparing the two electrode types since neural prosthetics control muscle movements by inducing tetanic contractions instead of twitches. If instead we compare the forces produced by tetanic stimuli, ISMS was as effective as whole nerve stimulation at producing strong forces. This would indicate only one site is required in the quadriceps pool to match whole nerve stimulation.

In either case, a measure of redundancy should be instituted leading to the implantations of two or more electrode shafts. This would provide a total of eight or more sites in each quadriceps pool. Separation between shafts in the RC direction (easier than implanting sites in the ML direction) should be 21% greater than the electrode site spacing in the DV direction. Since forces were found to be greater in the caudal half of the pool, the electrode shafts should be implanted between the motor pool's center and the caudal end.

The lack of a significant difference in the Ks between the caudal and rostral ends of the cord suggests that the Ks may be generalizable throughout the other motor pools of the lumbosacral spinal cord. In order to provide greater forces (since pulse amplitude recruitment curves rarely plateaued) and to operate near the chronaxie, an improved stimulation system needs to be capable of providing pulse amplitudes between 5 and 800 μA with pulse durations kept shorter than 200 μs.

V. Conclusion

Cylindrical multielectrodes were proven to be useful as a tool in the stimulation of the ventral horn of the spinal cord. The electrodes were inserted easily and stimulus delivery led to force levels and recruitment curve slopes similar to or better than other electrode types. The cylindrical multielectrodes have the advantage of multiple electrode sites on a single shaft which proved very useful in studying overlap and current spread.

The properties of the spinal cord were interrogated. For the stimulation parameters used, pulse width modulated recruitment proved more efficient at low charge levels and pulse amplitude modulated recruitment at high charge levels. Current-distance constants were found to have directional sensitivity.

Future studies of cylindrical multielectrodes should investigate electrode performance during chronic implantation studies with emphasis on the stability of impedances, thresholds, force levels and recruitment curve slopes. Future studies of overlap testing should seek to determine the properties and root cause of order effect.

Appendix

Equations used in calculation of K.
Known:

I_1 current pulse amplitude through electrode site #1 (units = μA);

I_2 current pulse amplitude through electrode site #2 (units = μA);

d distance between electrode sites (units=mm).

Unknown:

K current-distance constant (units = $\mu\mathrm{A/mm}^2$)

$$R_1 = \sqrt{\frac{I_1}{K}}, \quad R_2 = \sqrt{\frac{I_2}{K}}$$

$$X_1 = \frac{R_1^2 + d^2 - R_2^2}{2d}, \quad X_2 = d - X_1$$

$$V_1 = \frac{4}{3}\pi R_1^3, \quad V_2 = \frac{4}{3}\pi R_2^3$$

$$V_1' = \frac{\pi}{3}(R_1 - X_1)^2(2R_1 + X_1),$$

$$V_2' = \frac{\pi}{3}(R_2 - X_2)^2(2R_2 + X_2)$$

$$\text{Overlap} = \frac{V_1 \cap V_2}{V_1 \cup V_2} = \frac{V_1' + V_2'}{V_1 + V_2 - V_1' - V_2'}$$

Acknowledgment

The authors would like to thank Dr. S. Jacobsen for use of electrode microfabrication facilities, Dr. E. Lam and H. Rowland for production of radiographs, Dr. S. Lawrence for microfabrication process improvements, Dr. A. Prochazka for radiology suggestions, and Dr. J. Norton for advice on cuff electrode fabrication.

References

[1] Anon, "Spinal cord injury: facts and figures at a glance," *J. Spinal Cord Med.*, vol. 24, pp. 212–213, 2001.

[2] M. Sharma, E. B. Marsolais, G. Polando, R. J. Triolo, J. A. J. Davis, N. Bhadra, and J. P. Uhlir, "Implantation of a 16-channel functional electrical stimulation walking system," *Clin. Orthop.*, vol. 347, pp. 236–242, 1998.

[3] Z. Fang and J. T. Mortimer, "Selective activation of small motor axons by quasitrapezoidal current pulses," *IEEE Trans. Biomed. Eng.*, vol. 38, no. 2, pp. 168–174, Feb. 1991.

[4] A. Branner and R. A. Normann, "A multielectrode array for intrafascicular recording and stimulation in sciatic nerve of cats," *Brain Res. Bull.*, vol. 51, pp. 293–306, 2000.

[5] N. Nannini and K. Horch, "Muscle recruitment with intrafascicular electrodes," *IEEE Trans. Biomed. Eng.*, vol. 38, no. 8, pp. 769–776, Aug. 1991.

[6] D. Burke, R. Hicks, and J. Stephen, "Anodal and cathodal stimulation of the upper-limb area of the human motor cortex," *Brain*, vol. 115, pp. 1497–1508, 1992.

[7] R. S. Waters, D. D. Samulack, R. W. Dykes, and P. A. McKinley, "Topographic organization of baboon primary motor cortex: face, hand, forelimb, and shoulder representation," *Somatosens. Motor Res.*, vol. 7, pp. 485–514, 1990.

[8] V. K. Mushahwar and K. W. Horch, "Selective activation of muscle groups in the feline hindlimb through electrical microstimulation of the ventral lumbo-sacral spinal cord," *IEEE Trans. Rehabil. Eng.*, vol. 8, no. 1, pp. 11–21, Mar. 2000.

[9] R. Kobetic, R. J. Triolo, J. P. Uhlir, C. Bieri, M. Wibowo, G. Polando, E. B. Marsolais, J. A. J. Davis, and K. A. Ferguson, "Implanted functional electrical stimulation system for mobility in paraplegia: a follow-up case report," *IEEE Trans. Rehabil. Eng.*, vol. 7, no. 4, pp. 390–398, Dec. 1999.

[10] V. K. Mushahwar, D. F. Collins, and A. Prochazka, "Spinal cord microstimulation generates functional limb movements in chronically implanted cats," *Exp. Neurol.*, vol. 163, pp. 422–429, 2000.

[11] Y. Aoyagi, V. K. Mushahwar, R. B. Stein, and A. Prochazka, "Movements elicited by electrical stimulation of muscles, nerves, intermediate spinal cord, and spinal roots in anesthetized and decerebrate cats," *IEEE Trans. Neural Syst. Rehabil. Eng.*, vol. 12, no. 1, pp. 1–11, Mar. 2004.

[12] V. K. Mushahwar, D. M. Gillard, M. J. Gauthier, and A. Prochazka, "Intraspinal micro stimulation generates locomotor-like and feedback-controlled movements," *IEEE Trans. Neural Syst. Rehabil. Eng.*, vol. 10, no. 1, pp. 68–81, Mar. 2002.

[13] M. A. Lemay and W. M. Grill, "Modularity of motor output evoked by intraspinal microstimulation in cats," *J. Neurophysiol.*, vol. 91, pp. 502–514, 2004.

[14] A. Branner, R. B. Stein, and R. A. Normann, "Selective stimulation of cat sciatic nerve using an array of varying-length microelectrodes," *J. Neurophysiol.*, vol. 85, pp. 1585–1594, 2001.

[15] P. S. Motta and J. W. Judy, "Multielectrode microprobes for deep-brain stimulation fabricated using a novel 3-d shaping electroplating process," presented at the Digital Solid-State Sensor and Actuator Workshop, Hilton Head Island, SC, , 2002.

[16] V. K. Mushahwar and K. W. Horch, "Proposed specifications for a lumbar spinal cord electrode array for control of lower extremities in paraplegia," *IEEE Trans. Neural Syst. Rehabil. Eng.*, vol. 15, no. 3, pp. 237–243, Sep. 1997.

[17] S. Snow, S. C. Jacobsen, D. L. Wells, and K. W. Horch, "Microfabricated cylindrical multielectrodes for neural stimulation," *IEEE Trans. Biomedical Eng.*, vol. 53, no. 2, pp. 320–326, Feb. 2005.

[18] E. J. Tehovnik, "Electrical stimulation of neural tissue to evoke behavioral responses," *J. Neurosci. Meth.*, vol. 65, pp. 1–17, 1996.

[19] S. D. Stoney Jr., W. D. Thompson, and H. Asanuma, "Excitation of pyramidal tract cells by intracortical microstimulation: effective extent of stimulating current," *J. Neurophysiol.*, vol. 31, pp. 659–669, 1968.

[20] K. Yoshida and K. Horch, "Selective stimulation of peripheral nerve fibers using dual intrafascicular electrodes," *IEEE Trans. Biomed. Eng.*, vol. 40, no. 5, pp. 492–494, May 1993.

[21] R. E. Burke, D. N. Levine, M. Salcman, and P. Tsairis, "Motor units in cat soleus muscle: physiological, histochemical and morphological characteristics," *J. Physiol.*, vol. 238, pp. 503–514, 1974.

[22] C. Ghez, "Muscles," in *Principles of Neural Science*, 3rd ed, E. R. Kandel, Ed. New York: Elsevier, 1991, pp. 548–563.

[23] J. Bamford, C. T. Putman, and V. K. Mushahwar, "Intraspinal microstimulation preferentially recruits fatigue-resistant muscle fibres and generates gradual force in rat," *J. Physiol.*, pp. 873–884, 2005.

[24] V. K. Mushahwar and K. W. Horch, "Muscle recruitment through electrical stimulation of the lumbo-sacral spinal cord," *IEEE Trans. Neural Syst. Rehabil. Eng.*, vol. 8, no. 1, pp. 22–29, Mar. 2000.

[25] D. B. McCreery, W. F. Agnew, T. G. H. Yuen, and L. Bullara, "Charge density and charge per phase as cofactors in neural injury induced by electrical stimulation," *IEEE Trans. Biomed. Eng.*, vol. 37, no. 10, pp. 996–1000, Oct. 1990.

[26] H. Asanuma, A. Arnold, and P. Zarzecki, "Further study on the excitation of pyramidal tract cells by intracortical microstimulation," *Exp. Brain Res.*, vol. 26, pp. 443–461, 1976.

[27] J. B. J. Ranck, "Which elements are excited in electrical stimulation of mammalian central nervous system: a review," *Brain Res.*, vol. 98, pp. 417–440, 1975.

Sean Snow (S'02–M'05) received the B.E.E. degree in electrical engineering from Georgia Institute of Technology, Atlanta, in 1992 and the Ph.D. degree in bioengineering from the University of Utah, Salt Lake City, in 2005.

He served in the U.S. Peace Corps from 1992 to 1994 teaching physics in the Fiji Islands. He worked from 1995 to 1998 at Nikon Precision Inc., Belmont, CA, installing step-and-repeat systems for industrial photolithography applications.

Dr. Snow was awarded the Whitaker Foundation Graduate Fellowship from 1999 to 2004.

Kenneth W. Horch (M'88) received the B.S. degree from Lehigh University, Bethlehem, PA, and the Ph.D. degree from Yale University, New Haven, CT.

He is currently Professor of Bioengineering and Professor of Physiology at the University of Utah, Salt Lake City,

Dr. Horch is an AIMBE Fellow. For more information visit http://www.bioen.utah.edu/faculty/KWH.

Vivian K. Mushahwar (S93–M'96) received the B.Sc. degree in electrical engineering from Brigham Young University, Provo, UT, in 1991 and the Ph.D. degree in bioengineering from the University of Utah, Salt Lake City, in 1996. She received postdoctoral training at the Center for Rehabilitation Medicine at Emory University, Atlanta, GA, and the Center for Neuroscience at the University of Alberta, Edmonton, AB, Canada.

She is currently an Assistant Professor with the Department of Biomedical Engineering, University of Alberta, Edmonton, AB, Canada. Her work focuses on the development of rehabilitation interventions for restoring function to individuals with spinal cord injury, head trauma, and stroke.

Dr. Mushahwar is a member of IEEE EMBS Society, the International Functional Electrical Stimulation Society, the International Society for Magnetic Resonance in Medicine, the Society for Neuroscience, and the New York Academy of Science.